doi:10.3788/gzxb20154401.0113001

两节推挽极化波导 Y 型耦合器电光开关特性分析

李祝博[1],黄小亮[2],李翠婷[2],郑传涛[2]
(1 清华大学 微电子学研究所,北京,100084)
(2 集成光电子学国家重点联合实验室吉林大学实验区,吉林大学 电子科学与工程学院,长春 130012)

摘 要:针对两节独立反相集总电极聚合物 Y 型耦合器电光开关响应速度慢的问题,通过对该器件两节电光区的波导进行推挽极化,设计了一种无偏置行波电极高速电光开关.为了获得低的驱动电压、良好的阻抗匹配和光波与微波间较小的折射率失配,对电极参数做了设计和优化.通过对施加的方波开关信号做傅里叶变换并结合行波传输线理论,给出了一种用于建模和表征器件高频响应的解析分析法.对该器件的数值计算结果表明,在 1 550 nm 中心工作波长下,其 3 dB 状态电压为 0 V,开关电压为 2.68 V,上分支状态电压和下分支状态电压分别为 −1.34 V 和 +1.34 V,器件的插入损耗和串扰分别小于 3.55 和 −30 dB,10%～90%上升时间和下降时间均为 3.90 ps,截止开关频率可达 128.2 GHz.

关键词:集成光学;导波光学;聚合物;电光开关
中图分类号:TN253 **文献标识码**:A **文章编号**:1004-4213(2015)01-0113001-6

Characteristics of a Y-fed Coupler Electro-optic Switch Using Two-section Push-pull Poled Waveguides

LI Zhu-bo[1], HUANG Xiao-liang[2], LI Cui-ting[2], ZHENG Chuan-tao[2]
(1 *Institute of Microelectronics, Tsinghua University, Beijing* 100084, *China*)
(2 *State Key Laboratory on Integrated Optoelectronics, College of Electronic Science and Engineering, Jilin University, Changchun* 130012, *China*)

Abstract: Considering that the switching speed of the Y-fed coupler Electro-Optic (EO) switch with two-section seperated reversed lumped electrodes is slow, through push-pull poling on the wavegides in the two EO regions, a bias-free high-speed travelling-wave line EO switch was designed. Design and optimization were performed on electrode parameters for obtaining low driving voltage, good impedance match and less-mismatch between optical index and microwave index. Besides, by using Fourier transformation on the applied square-wave switching signal, a novel analytical technique was presented to model and characterize the switching response. Numerical calculation results of the optimized device indicate that, under 1 550 nm central operation wavelength, the 3 dB state voltage is 0 V, and the upper- and lower-branch state voltages are −1.34 V and +1.34 V, respectively, indicating a switching voltage of 2.68 V. The insertion loss and crosstalk are less than 3.55 and −30 dB, respectively, and the 10%～90% rise time and fall time are both about 3.90 ps, indicating a cutoff switching frequency up to 128.2 GHz. The proposed high-speed device structre and numerical technique are of well meaning for the design and performance evaluation of a similar device based on Y-fed coupler structure.

Key words: Integrated optics; Guided-wave optics; Polymer; Electro-optic switch
OCIS Codes: 130.0130; 130.2790; 130.5460; 230.7370; 230.3120; 250.5460

Foundation item: The National Natural Science Foundation Council of China (No. 61107021), the Ministry of Education of China (Nos. 20110061120052 and 20120061130008), the Science and Technology Department of Jilin Province of China (No. 20130522161JH), and the Special Funds of Basic Science and Technology of Jilin University (No. 201103076)

First author: LI Zhu-bo (1992−), male, master candidate, mainly focuses on micrometer electro−optic devices. Email: zyf_jc@163.com
Supervisor (Contact author): ZHENG Chuan-tao (1982−), male, Associate Professor, Ph. D. degree, mainly focuses on guided−wave optics and optoelectronics. Email: zhengchuantao@jlu.edu.cn

Received: Jun. 25, 2014; **Accepted**: Aug. 20, 2014

0 Introduction

As Silicon-On-Insulator (SOI) Electro-Optic (EO) modulators/switches based on carrier-injection effect [1-3], poled polymer EO modulators/switches are also vital components in optical communication systems, optical sensors, optical computers, etc, and various EO devices based on different waveguide structures (Y-fed coupler, Directional Coupler (DC), Mach-Zehnder Interferometer (MZI), etc), electrode structures (Microstrip Line (MSL), Coplanar Waveguide (CPW), $\Delta\beta$-reversal, etc), and fabrication technologies have been reported [4-8]. In recent years, for obtaining low driving voltage, low insertion loss and crosstalk, fast switching speed and wide spectrum, different EO switches [9-11], which can also be served as EO modulators, have also been demonstrated theoretically or experimentally.

In 2009, a $\Delta\beta$-reversal Y-fed coupler EO switch[12] was reported by adopting two-section separated electrodes, and its 3-dB modulation bandwidth or cutoff switching frequency cannot be too high, because the device cannot be configured to be traveling-wave style. In our recent report, for enabling the $\Delta\beta$-reversal standard DC EO switch working at traveling-wave style, a CPW grounded (CPWG) electrode was used[13], where both two waveguide cores in the two EO sections are uniformly poled along the same direction. Alternatively, for the Y-fed coupler device in this paper, only one waveguide core in each section is poled, and hereby a push-pull poled traveling-wave Y-fed coupler EO switch using non-bending uniform MSL electrode was demonstrated, and through optimization, this modulator reveals a high cut-off switching frequency up to 128.2 GHz. The differences between this electrode structure and that reported in Ref. [13] are: 1) only one signal electrode is required, but in Ref. [13], one signal electrode and two grounded electrodes are all required; 2) because the two waveguide sections in this paper are push-pull poled, the electrode need not be bent for resulting in phase mismatch between two sections; in Ref. [13], because the two waveguide sections are uniformly poled, the signal electrode should be bent to move from one waveguide to another, for generating phase mismatch between the two sections.

Besides that, for investigating switching characteristics for the proposed device at its design stage, a formulation technique was presented in this paper. The basic concept of this technique is that for a driving signal with any form, the instantaneous applied voltage along the electrode can be treated as the superposition of definite or infinite amount of harmonic signals, and the total transfer matrix was achievable through the numerical integration on micro transfer matrix during the whole propagation process of an optical microelement.

1 Device structure

Fig. 1(a) shows the schematic diagram of the polymer Y-fed coupler EO modulator with traveling-wave MSL electrode and push-pull poled waveguide sections. A Y-branch splitting waveguide is utilized in the input region, and the input power and amplitude are defined as P_{in} and R_{in}, respectively. Two identical parallel rib waveguides with a total length L are used in the EO active region, and their coupling distance is d. The EO region is divided into two sections, and each section has a length of $L/2$. The output power from the upper waveguide and that from the under waveguide are P_{1out} and P_{2out}, respectively, and the corresponding light amplitudes are R_{out} and S_{out}, respectively. For increasing modulation bandwidth, the driving electrode is configured as distributed traveling-wave style. The input time-variation Radio-Frequency (RF) signal is $u(t)$, and the load impedance is Z_L.

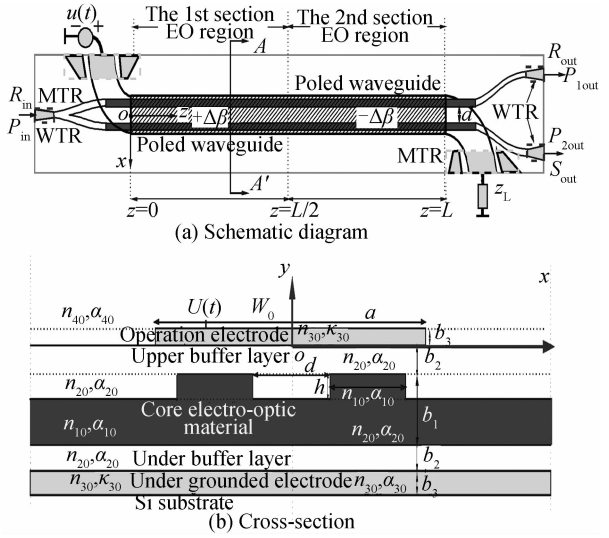

Fig. 1 Structure of the polymer Y-fed coupler EO modulator with traveling-wave MSL electrode and push-pull poled waveguide sections. WTR: waveguide transitive region; MTR: microwave transitive region

The cross-section view AA′ in the EO section region is shown in Fig. 1(b), and the driving electrode includes the upper operation electrode and the under grounded electrode. The structure of the rib waveguide is as: air/upper electrode/upper buffer layer/core/under buffer layer/under electrode/substrate, where only the core is EO material. Let W_0 be the width of the central operation electrode, and b_3 be the thickness of the upper and under electrodes. For the rib waveguide, the core width, rib height and core thickness are a, h

and b_1, respectively. The thickness of the upper/under buffer layers is b_2.

2 Parameter optimization

2.1 Basic parameters

Under 1 550 nm, the refractive index, bulk amplitude attenuation coefficient and EO coefficient of the Diels-Alder cross-linkable EO core polymer AJ309 are $n_{10}=1.643$, $\alpha_{10}=2.0$ dB/cm, and $\gamma_{33}=138$ pm/V, respectively [14-15]. The refractive index and bulk amplitude attenuation coefficient of the upper and under buffer layers and the cladding beside the core PFS-GMA are $n_{20}=1.461$ and $\alpha_{20}=0.25$ dB/cm[16], and those of the confined layer air are $n_{40}=1.0$ and $\alpha_{40}=0$ dB/cm, respectively. The refractive index and bulk extinction coefficient of the gold electrode are $n_{30}=0.19$ and $\kappa_{30}=6.1$, respectively [17]. The parameters are optimized as: $a=4.0$ μm, $b_1=1.5$ μm, $h=0.5$ μm, $b_2=1.5$ μm, and $b_3\geqslant 0.10$ μm,. The calculated E_{00}^y mode loss coefficient is about $\alpha_P=2.32$ dB/cm, and its effective refractive index is about $n_{eff0}=1.593\,6$.

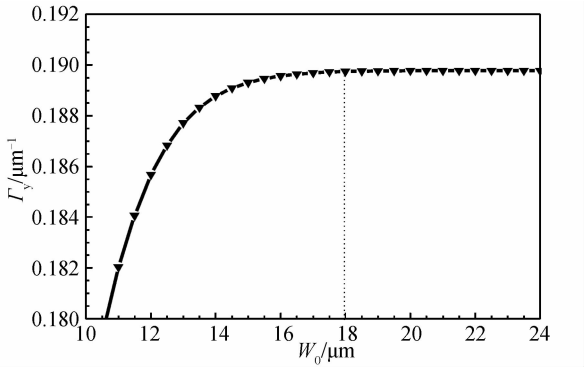

Fig. 2 Curves of Γ_y versus W_0 where $b_3=0.1$ μm

2.2 EO overlap integral

For the lower waveguide core in the first section or the upper waveguide core in the second section, the EO overlap integral along the y-direction can be described as

$$\Gamma_y=\frac{\iint_{EO_{core}}\frac{1}{U}E_y(x,y)\,|E_{optic}(x,y)|^2\,dxdy}{\iint_{-\infty\sim+\infty}|E_{optic}(x,y)|^2\,dxdy} \tag{1}$$

where $E_{optic}(x,y)$ is the E_{00}^y mode optical field distribution, and $E_y(x,y)$ is the applied electric field component along y direction which can be analyzed by using point-matching method [18]. Fig. 2 exhibits the curve of Γ_y versus W_0, where $d=3.0$ μm and $b_3=0.10$ μm. It can be found that as W increases, Γ_y increases in magnitude, so a larger W_0 is required. However, when $W_0\geqslant 18$ μm, Γ_{eq}^y changes slightly.

2.3 Microwave parameters

On another aspect, a microwave impedance (Z_c) of 50 Ω and a less mismatch between microwave index (n_m) and lightwave index (n_{eff0}) are both demanded for realizing normal high-frequency modulation performance. For the electrode structure shown in Fig. 1(b), Fig. 3 shows the curves of (a) n_m and (b) Z_c versus W_0, where $d=3.0$ μm, and $b_3=0.1$ μm. From Fig. 3 (b), to realize the impedance match among electric coaxial cable, electrode and load impedance, we choose $W_0=14.0$ μm. The corresponding microwave parameters are $n_m=1.401\,0$ and $Z_c=50.2$ Ω. From Fig. 2, when $W_0=14.0$ μm, we have $\Gamma_y=0.19$ μm^{-1}.

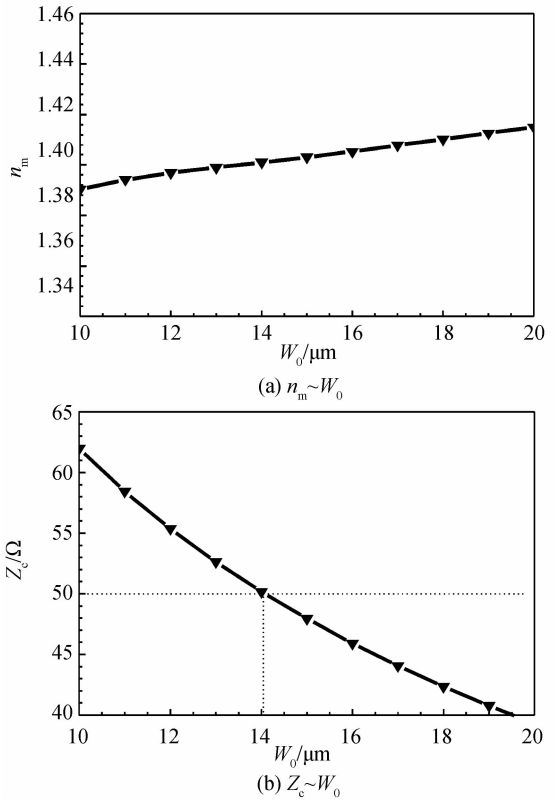

Fig. 3 Curves of n_m and Z_c versus W_0 where $S_0=50$ μm and $b_3=0.1$ μm

3 Static characteristics analysis

In the first section, only the lower waveguide is poled, and the change of mode effective index is

$$\Delta n_{eff2}(U)=-\frac{n_{10}^3}{2}\gamma_{33}U\Gamma_y \tag{2}$$

Then the propagation constant mismatch between the lower waveguide and the upper waveguide is $\Delta\beta^1=\beta_2^1-\beta_1^1=k_0\Delta n_{eff2}$. In the second section, since only the upper waveguide is poled, the change of its mode effective index is

$$\Delta n_{eff1}(U)=-\frac{n_{10}^3}{2}\gamma_{33}U\Gamma_y \tag{3}$$

Then the propagation constant mismatch between the under waveguide and the upper waveguide is $\Delta\beta^2=\beta_2^2-\beta_1^2=-k_0\Delta n_{eff1}$. Since $\Delta n_{eff1}=\Delta n_{eff2}=\Delta n_{eff}$, let $\Delta\beta^1=+\Delta\beta$ for the first EO section and $\Delta\beta^2=-\Delta\beta$ for the second EO section.

Let K be the coupling coefficient between two directional coupling waveguides, and $L_0=\frac{\pi}{2K}$ be the coupling length of the directional coupler. For convenience in the following analysis, we introduce two amplitude transfer matrices $T^+(u,v)$ and $T^-(u,v)$, corresponding to the first waveguide section and the second waveguide section, as

$$T^+(u,v)=\begin{pmatrix} A(u,v) & -\mathrm{j}B(u,v) \\ -\mathrm{j}B^*(u,v) & A^*(u,v) \end{pmatrix} \tag{4}$$

$$T^-(u,v)=\begin{pmatrix} A^*(u,v) & -\mathrm{j}B(u,v) \\ -\mathrm{j}B^*(u,v) & A(u,v) \end{pmatrix} \tag{5}$$

where $A(u,v)=\cos\left(\frac{\pi}{4}\sqrt{u^2+v^2}\right)+\mathrm{j}\frac{v}{\sqrt{u^2+v^2}}\cdot\sin\left(\frac{\pi}{4}\sqrt{u^2+v^2}\right)$ and $B(u,v)=\frac{u}{\sqrt{u^2+v^2}}\cdot\sin\left(\frac{\pi}{4}\sqrt{u^2+v^2}\right)$. The output light amplitudes from the upper/lower branches can be expressed as

$$\begin{pmatrix} R_{\mathrm{out}} \\ S_{\mathrm{out}} \end{pmatrix}=T^-(u,v)T^+(u,v)\begin{bmatrix} R_{\mathrm{in}}/\sqrt{2} \\ R_{\mathrm{in}}/\sqrt{2} \end{bmatrix}\equiv \begin{pmatrix} M(u,v) & -\mathrm{j}N(u,v) \\ -\mathrm{j}N^*(u,v) & M^*(u,v) \end{pmatrix}\begin{bmatrix} R_{\mathrm{in}}/\sqrt{2} \\ R_{\mathrm{in}}/\sqrt{2} \end{bmatrix} \tag{6}$$

$$M(u,v)=|A(u,v)|^2-|B^*(u,v)|^2 \tag{7}$$

$$N(u,v)=A^*(u,v)B(u,v)+A^*(u,v)B(u,v) \tag{8}$$

where $u=L/L_0$ and $v=\Delta\beta L/\pi$. Therefore, the output powers from the upper/lower branches are determined as, respectively

From the discussion in Ref. [9], in order to realize perfect switching operation with the minimum crosstalk, it is desired that $u=\sqrt{2+\sqrt{2}}$, and another variable v can be treated as a function of the applied voltage U, that is,

$$v(U)=k_0\Delta n_{\mathrm{eff}}(U)L/\pi \tag{9}$$

where Δn_{eff} is given by Eqs. (2) and (3). Then the static response can be determined as

$$P_{1\mathrm{out}}^{\mathrm{DC}}(L=uL_0,U)= 10\lg\left(\frac{1}{2}|M(u,v)-\mathrm{j}N(u,v)|^2\right)-2\alpha_{\mathrm{p}}L_{\mathrm{total}} \tag{10}$$

$$P_{2\mathrm{out}}^{\mathrm{DC}}(L=uL_0,U)= 10\lg\left(\frac{1}{2}|-\mathrm{j}N^*(u,v)+M^*(u,v)|^2\right)-2\alpha_{\mathrm{p}}L_{\mathrm{total}} \tag{11}$$

Fig. 4 exhibits the curves of the output powers $P_{1\mathrm{out}}$ and $P_{2\mathrm{out}}$ versus the applied direct-current voltage U, where $d=3.0$ μm, $b_3=0.10$ μm, $W_0=14$ μm, and $L=\sqrt{2+\sqrt{2}}L_0=7.648$ mm. It can be found that when the applied voltage is $U=1.34$ V, the output power from the upper branch becomes the maximum, while that from the lower branch becomes the minimum; when the applied voltage is $U=-1.34$ V, the output power from the upper branch becomes the minimum, while that from the lower branch becomes the maximum. Therefore, the half-wave voltage of the modulator is determined to be $U_\pi=2.68$ V. Under the operation voltages of $\pm U_\pi/2$, the insertion loss under ON state is less than 3.55 dB, and the crosstalk between OFF and ON states is less than −30 dB.

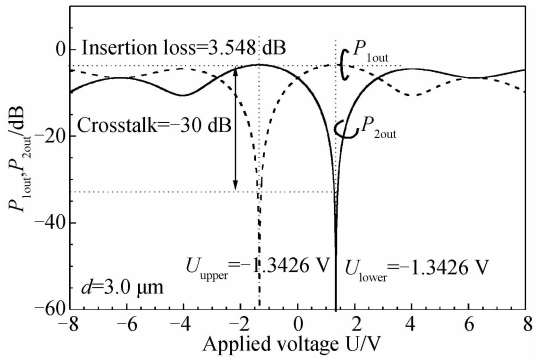

Fig. 4 Curves of $P_{1\mathrm{out}}$ and $P_{2\mathrm{out}}$ versus U

4 Dynamic characteristics analysis

Suppose a biased square-wave signal is used to operate the device, and let its frequency, amplitude and duty cycle be f_{m}, U_{g} and 1/2, separately. Based on Fourier transformation, such signal can be expanded to a series of harmonic cosine-wave signals, as

$$u_{\mathrm{squ}}(t)=U_{\mathrm{g}}\sum_{n=1}^{\infty}\frac{\sin(n\pi/2)}{n\pi/2}\cos\left[2\pi(nf_{\mathrm{m}})t\right] \tag{12}$$

We can see that $u_{\mathrm{squ}}(t)$ contains infinite components with different frequencies. In the EO active region, define the lightwave velocity as $v_{\mathrm{c}}=c/n_{\mathrm{eff0}}$. The lightwave microelement that inputs into $z=0$ at t will experience two stages before output from the waveguide at $z=L$ and $t+L/v_{\mathrm{c}}$. There are two stages analyzed below

1) In the first electrode section region during $t\leqslant t'<t+L/(2v_{\mathrm{c}})$, the electrode and the waveguide are parallel. At the moment t′, the position of the lightwave element is

$$z_1(t')=(c/n_{\mathrm{eff0}})(t'-t) \tag{13}$$

and the applied voltage at $z_1(t')$ is

$$u[z_1(t'),t']=U_g\sum_{n=1}^{\infty}\left\{\frac{\sin(n\pi/2)}{n\pi/2}\times\cos\left[2\pi(nf_m)t'-\frac{2\pi(nf_m)n_m}{c}z_1(t')\right]\right\} \tag{14}$$

So the amplitude transfer matrix of the first electrode section can be obtained as

$$T_1(u[z_1(t'),t'])\Big|_{t'=t}^{t'=t+(L/2)/v_{\mathrm{c}}}=\lim_{\Delta t\to 0}\prod_{t'=t}^{t+(L/2)/v_{\mathrm{c}}}T^+\left[v_{\mathrm{c}}\Delta t/L_0,\Delta\beta(u[z_1(t'),t'])v_{\mathrm{c}}\Delta t/\pi\right] \tag{15}$$

where $\Delta\beta(u[z_1(t'),t'])=\Delta\beta^{\mathrm{l}}$.

2) In the second electrode section region during $t+(L/2)/v_{\mathrm{c}}\leqslant t'<t+L/v_{\mathrm{c}}$, the position of the lightwave element is

$$z_2(t') = L/2 + v_c[t' - (L/2)/v_c] \tag{16}$$

and the applied voltage at $z_1(t')$ is

$$u[z_1(t'), t'] = U_g \sum_{n=1}^{\infty} \left\{ \frac{\sin(n\pi/2)}{n\pi/2} \times \cos[2\pi(nf_m)t' - [2\pi(nf_m)n_m/c]z_1(t')] \right\} \tag{17}$$

Then the transfer matrix T_2 in this region can be expressed as

$$T_2(u[z_2(t'), t'])_{t'=t+(L)/v_c}^{t'=t+(L/2)/v_c} = \lim_{\Delta t \to 0} \prod_{t'=t+(L/2)/v_c}^{t+L/v_c} T^- \left[\frac{v_c \Delta t}{L_0}, \frac{\Delta\beta(u[z_2(t'), t'])v_c \Delta t}{\pi} \right] \tag{18}$$

where $\Delta\beta(u[z_1(t'), t']) = \Delta\beta^2$.

Therefore, the dynamic transfer matrix of the switch related to t can be written as

$$T_{dyn}[t + L/v_c] = T_2 \times T_1 = \begin{pmatrix} M_{dyn}(t) & -jN_{dyn}(t) \\ -jN_{dyn}^*(t) & M_{dyn}^*(t) \end{pmatrix} \tag{19}$$

where M_{dyn} and N_{dyn} are achieved from numerical integration, and the baseband responses are

$$P_{1out}^{dyn}(t) = 20\lg |M_{dyn}(t - L/v_c)| - 2\alpha L_{total} \tag{20}$$

$$P_{2out}^{dyn}(t) = 20\lg |N_{dyn}^*(t - L/v_c)| - 2\alpha L_{total} \tag{21}$$

Under the modulation of square-wave signal, Fig. 5 shows the calculated results of (a) the time-domain response for one period as well as (b) the detailed response for the rise and fall edges under f_m = 10 MHz, and (c) the time-domain response for two periods as well as (d) the detailed response for the fall edge under f_m = 10 GHz, where 400 harmonic frequency components are considered in the Fourier expansion of each square-wave signal, $U_g = U_\pi/2$. We find from Figs. 5(a) and 5(c) that the driving signal does not changes in a step style, because definite amounts of harmonic components are used to form the signal. To further decide switching response parameters, we use a 10 GHz square-wave signal to operate the device (shown in Figs. 5(b) and 5(d)), the 10%～90% rise time and fall time are both determined to be about t_{rise}, t_{fall} = 3.90 ps, and the switching time is t_s = 40.2 ps. So the cutoff switching frequency can be estimated to be about

$$f_{cut}^m = \frac{1}{(t_{rise} + t_{fall})} = 128.2 \text{ GHz} \tag{22}$$

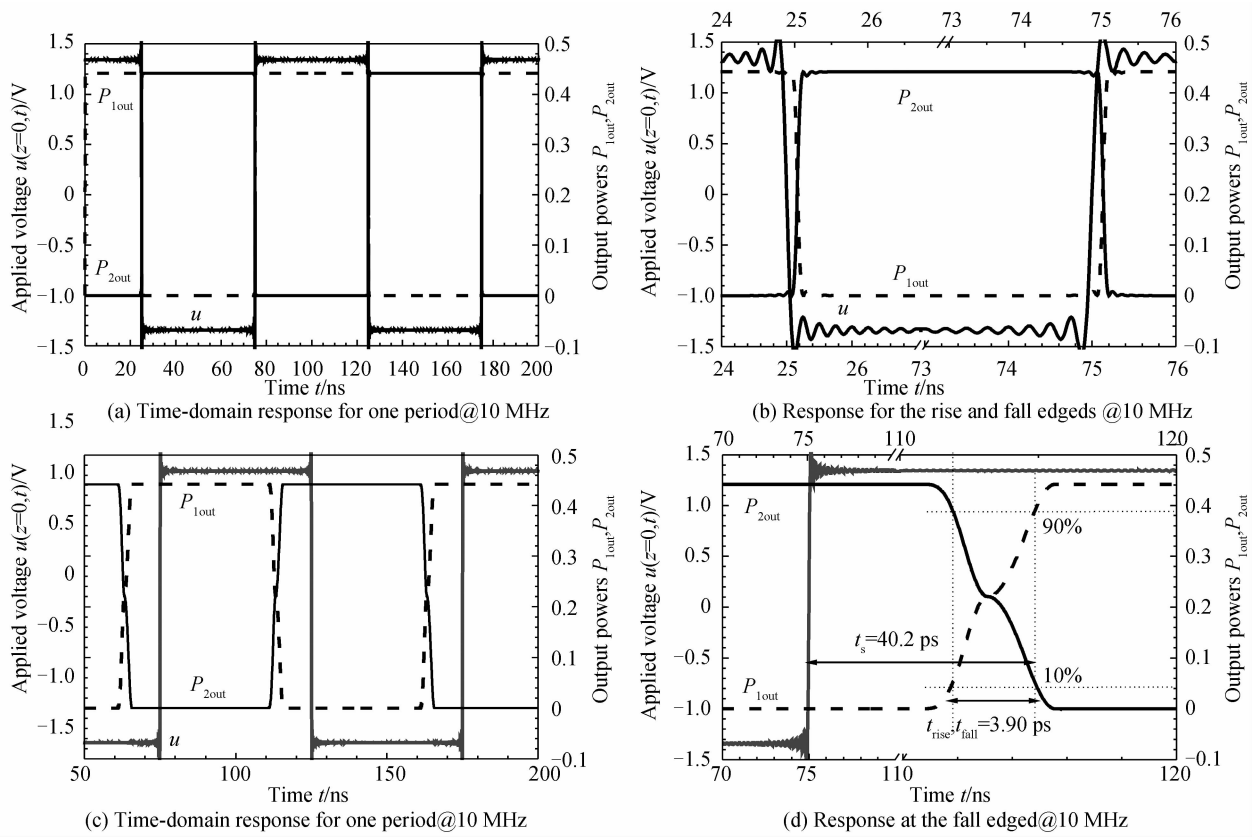

Fig. 5 Time-domain responses under 10 MHz and 10 GHz switching operations

5 Conclusions

Through push-pull poling on a selective waveguide core in each EO section, a polymer Y-fed coupler EO switch with traveling-wave driving configuration was proposed. Both the waveguide and electrode parameters were thoroughly optimized. Analytical results under 1 550 nm reveal that, its upper-branch and lower-branch state voltages are ± 1.34 V, respectively, and the insertion loss and crosstalk are less than 3.55 and −30 dB, respectively. The results show that the modulator possesses a cutoff switching frequency up to 128.2 GHz. The 10～90% rise time and fall time are both about 3.90 ps. The switch shows potential

application in on-chip communication networks due to its bias-free function and high cut-off switching frequency.

Reference

[1] VLASOV Y, GREEN W M J, XIA F. High-throughput silicon nanophotonic wavelength-insensitive switch for on-chip optical networks [J]. *Nature Photonics*, 2008, **2**(4): 242-246.

[2] TAKAHASHI K, KANAMORI Y, KOKUBUN Y, *et al*. A wavelength-selective add-drop switch using silicon microring resonator with a submicron-comb electrostatic actuator [J]. *Optics Express*, 2008, **16**(19): 14421-14428.

[3] WEI Li-ping, WANG Yong-hua, ZANG Jun-bin, *et al*. Analysis and optimum design of silicon-on-insulator micro-ring resonator electro-optic modulator [J]. *Acta Photonica Sinica*, 2013, **42**(12): 1473-1477.

[4] LI Ran, WANG Lei, CHEN Xi, *et al*. Design of an integrated device of delay line array and thermal optical switch based on polymeric materials [J]. *Acta Photonica Sinica*, 2014, **43**(4): 0423002.

[5] ZHENG Chuan-Tao, LUO Qian-Qian, *et al*. Polymer electro-optic switch using cross-coupling five-serial-coupled microring resonator with ultra-low crosstalk [J]. *Acta Photonica Sinica*, 2014, **43**(3): 0313001.

[6] ENAMI Y, MATHINE D, DEROSE CT, *et al*. Hybrid electro-optic polymer/sol-gel waveguide directional coupler switches [J]. *Applied Physics Letters*, 2009, **94**(21): 213513.

[7] CHEN C, ZHANG F, WANG H, *et al*. UV curable electro-optic polymer modulator based on direct photo definition technique [J]. *IEEE Journal of Quantum Electronics*, 2011, **47**(7): 959-964.

[8] BALAKRISHNAN M, FACCINI M, DIEMEER M B J, *et al*. Microring resonator based modulator made by direct photodefinition of an electro-optic polymer [J]. *Applied Physics Letters*, 2008, **92**(15): 153310.

[9] ZHENG C T, MA C S, YAN X, *et al*. Simulation and optimization of a polymer directional coupler electro-optic switch with push-pull electrodes [J]. *Optics Communications*, 2008, **281**(14): 3695-3702.

[10] ZHENG C T, MA C S, YAN X, *et al*. Analysis of response characteristics for polymer directional coupler electro-optic switches [J]. *Optics Communications*, 2008, **281**(24): 5998-6005.

[11] ZHENG C T, MA C S, YAN X, *et al*. Design of integrated 1×2, 1×4 low driving voltage polymer electro-optic switches based on Y-fed directional couplers [J]. *Journal of Modern Optics*, 2009, **56**(5): 615-622.

[12] ZHENG C T, MA C S, YAN X, *et al*. Analysis and optimum design of a polymer Y-fed coupler electro-optic switch using double-section reversed electrodes [J]. *Journal of Modern Optics*, 2009, **56**(12): 1383-1391.

[13] WANG R, ZHENG CT, SONG Q, *et al*. Fourier analysis of a polymer directional coupler electro-optic switch with two-section cosine-transitive CPWG electrodes: A new theoretical view [J]. *Optics Communications*, 2012, **285**(6): 1103-1112.

[14] ENAMI Y, DEROSE CT, MATHINE D, *et al*. Hybrid polymer/sol-gel waveguide modulators with exceptionally large electro-optic coefficients [J]. *Nature Photonics*, 2007, **1**(3): 180-185.

[15] ENAMI Y, MATHINE D, DEROSE C T, *et al*. Hybrid cross-linkable polymer/sol-gel waveguide modulators with 0.65 V half wave voltage at 1550 nm [J]. *Applied Physics Letters*, 2007, **91**(9): 093505.

[16] PITOIS C, VUKMIROVIC C, HULT A, *et al*. Low-loss passive optical waveguides based on photosensitive poly (pentafluorostyrene-co-glycidyl methacrylate) [J]. *Macromolecules*, 1999, **32**(9): 2903-2909.

[17] DRISCOLL W G, VAUGHAN W, Handbook of Optics[M]. New York: McGraw-Hill, 1978, pp. 7.

[18] ZHU N H, QIU W, PUN E Y B, *et al*. Quasi-static analysis of shielded microstrip transmission lines with thick electrodes [J]. *IEEE Transaction on Microwave Theory and Technique*, 1997, **45**(2): 288-291.